XX IMEKO World Congress
Metrology for Green Growth
September 9-14, 2012, Busan, Republic of Korea.

DSP BASED READ OUT SYSTEM FOR CONTACTLESS HIGH–FREQUENCY INDUCTIVE POSITION SENSORS

B. Aschenbrenner, B. G. Zagar

Institute for Measurement Technology, Johannes Kepler University, Linz, Austria,
bernhard.aschenbrenner@jku.at bernhard.zagar@jku.at

Abstract — This paper presents a precise and low cost absolute position inductive measurement system for rough industrial environments. This transducer works on similar principles as contactless resolvers but consists of a rectangular antenna PCB, a passive LC resonance target and a signal processing unit. The read out electronics utilize undersampling to demodulate the transducer in–phase and quadrature output signals. Furthermore, the corresponding position is estimated from a lookup table (LUT) to avoid singularities in the inverse tangent and cotangent calculation. The mechanical transducer arrangement, signal condition electronics design and measured results will be presented.

Keywords — inductive sensor, contactless, undersampling, quadrature, synchronous demodulation

1. INTRODUCTION

Many industrial applications demand for precise absolute position measurement of objects in a harsh environment. Sensors for industrial applications have to meet criteria such as reliability, small size, wide temperature range, insensitivity to moisture, vibrations, dust, chemicals and mechanical offset even in rough conditions. Ideally, the measurement system should fulfill these criteria without any mechanical contact to maintain long service life and should be applicable for high dynamical drives.

Prime candidates to meet these requirements are contactless inductive sensors. One of these inductive sensors is based on inductive resonance [1–3]. The applied sensor can be used for absolute displacement measurement even in harsh environments and measures the position right from start up.

The introduced sensor works on a similar principle to contactless resolvers and utilizes the mutual inductance between an elongated antenna on a printed circuit board (PCB) and a target which acts as a resonance circuit. The principle operation is shown in Figure 1. The target is a passive high-Q resonant circuit formed by tracks on a PCB (L_T) and a capacitor (C_T) (see Figures 2 and 3). Furthermore, the antenna PCB contains five different planar coils which work as transmit and receive antennas. The sine and cosine coil pair with the period over the full antenna PCB length l_{th} is used for absolute position measurement and the other two coils with the period $l_{th}/9.75$ is used for increasing the position measurement precision, but are incremental. The amplitude modulated output voltages of the receiver coils contain the position information of the target. These voltages have to be demodulated and quantized to calculate the position on a DSP.

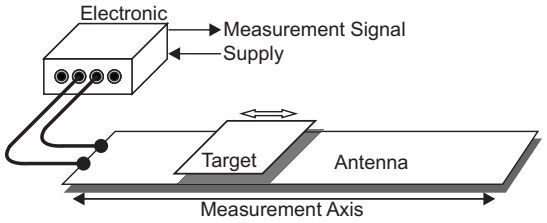

Fig. 1: Contactless inductive position sensor in linear arrangement, consisting of an antenna PCB, a movable high Q resonant circuit and a signal conditioning electronic.

Conventional resolver to digital converters seem to be ideal for high–frequency inductive position sensors but the carrier frequency of these converters, which is usually between 2 and 30 kHz, is too low. In [1, 4], an ASIC front end was developed for this kind of sensor which demodulates, amplifies and filters the in–phase and quadrature signals from the receiver coils and

provides an excitation voltage that supplies the transmitter coil, but the ASIC can not simultaneously sample the four receiver coil signals. This is necessary, however, for fast moving objects.

After this introductory part, Section 2 describes the basic theory of operation of the sensor. Section 3 describes the demodulation of the received sensor signals utilizing digital undersampling. Section 4 gives an overview of the already developed signal conditioning electronics and preliminary measurements. Finally, conclusions are suitably drawn in Section 5.

2. OPERATING PRINCIPLES

The inductive position sensor operating principle is similar to the resolver operating principle. However, instead of a rotor winding and two stator windings there are the transmit coil and four receive coils on the same antenna PCB. Furthermore, the coils are planar on the PCB instead of a spatial arrangement like the resolver windings in a motor stator.

A typically planar arrangement of tracks which forms transmit and receive circuits illustrates Figure 3. The transmit coil is formed by tracks which extend around the periphery of the PCB forming three loops. The sine-shaped tracks are the receive coils. Four coils with two different periods of both sine- and cosine-structures determine the target position (see Figure 3). The target is a simple passive serial LC resonant circuit whose Q-factor should be as high as possible. The inductance is formed by tracks on a PCB (see Figure 2). Targets are relative short compared to the stator antenna.

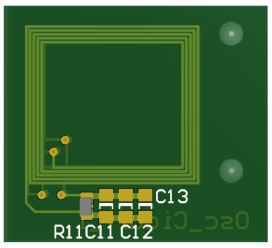

Fig. 2: Resonant target PCB with the rectangular planar coil windings to form the inductance for the serial LC resonant circuit

The two long pitched coils determine the absolute position. The fine pitched windings improve the transducer resolution but are incremental. Thus, the long pitched coils must resolve smaller displacements than half the period of the small pitched coils to obtain the correct incremental index. Consequently, the multiplication of the increment number and period length

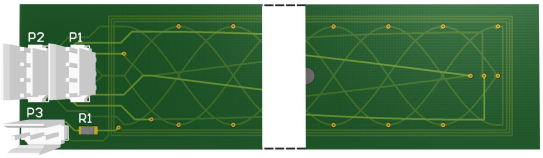

Fig. 3: The developed and manufactured antenna PCB can be seen with the excitation winding and the different sine and cosine structures which are manufactured on a four layer PCB. The illustrated sensor offers a theoretical absolute measurement length l_{th} of 390 mm

plus the relative target position delivers the precise and absolute target position. The combination of different pitches improves the transducer for high resolution position measurement.

Usually, a sine or square wave signal supplies the rectangular transmitter coil which has a frequency range between 100 kHz and 4 MHz [1] where the fundamental oscillation can be represented as $U_{Tx} = A_{Tx} \sin(2\pi f_0 t)$, where A_{Tx} and f_0 are the amplitude and the fundamental frequency of the excitation signal.

In the region of the transmitter coil, a uniform, elongated and alternating electromagnetic field is formed due to the excitation. When the target enters the alternating exciting field, currents are induced to flow in the resonant circuit. These currents generate their own flux field, which induces a voltage in the receiver coils. The magnetic coupling between the resonant circuit and each of the sensor windings varies with position, so that by applying an oscillating signal to the excitation winding at target resonant frequency, a signal is induced in the transducer winding which oscillates at the resonant frequency but whose amplitude varies as a function of the relative position of the antenna and the target PCB.

An in-phase signal and a quadrature signal (that is 90° out of phase to the in-phase signal) are measured at the receiver coils. The two amplitude modulated receiver signals from the absolute structure can be represented in the time domain as follows:

$$U_{Asin} = A_A \sin\left(\frac{2\pi x}{l_{th}}\right) \sin\left(\omega_0 + \frac{\pi}{2}\right), \quad (1)$$

$$U_{Acos} = A_A \cos\left(\frac{2\pi x}{l_{th}}\right) \sin\left(\omega_0 + \frac{\pi}{2}\right), \quad (2)$$

where x is the absolute position of the target along the measurement axis, l_{th} is the pitch of the antenna absolute position coils, and ω_0 is the angular speed of the target resonance and excitation voltage carrier frequency [1].

Furthermore, the two amplitude modulated receiver signals from the precise structure can be represented in the time domain as follows:

$$U_{Psin} = A_P \sin\left(\frac{2\pi x_P}{l_P}\right) \sin\left(\omega_0 + \frac{\pi}{2}\right), \quad (3)$$

$$U_{Pcos} = A_P \cos\left(\frac{2\pi x_p}{l_P}\right) \sin\left(\omega_0 + \frac{\pi}{2}\right), \quad (4)$$

where x_p is the precise but incremental position of the target and l_P is the pitch of the antenna precise position coils.

The target position is determined from the relative amplitudes of the components of the signal induced in the sensor windings corresponding to the in-phase and the quadrature signal. Because of the receive coils design, the signals in the coils due to the oscillating target flux are in phase with each other but are in quadrature as a function of position along the antenna PCB. The measured in-phase signal from the sine coil and the quadrature signal from the cosine coil are inputs to two simultaneous sampling analog to digital converter (ADC) which sample at the same frequency as the carrier frequency f_0. This, so called undersampling, synchronously demodulates and quantizes both analog signals.

A key characteristic of this sensor is that there is no hysteresis unlike in many other magnetic sensor designs, where hysteresis effects significantly increase in the magnetic field intensity and flux density curve. Furthermore, without the target circuit there are no induced currents in the receive windings, because the conductive tracks of the sine and cosine receive coils are arranged as balanced dipoles. Therefore, the electrical current induced by the exciting field to flow in one loop of the stator winding is canceled by an equal and opposite in phase induced current of the other loop. Using such balanced dipoles has the advantage that the influence by electromagnetic noise and inductive crosstalk of the exciting coil current becomes reduced.

Crosstalk is generally a cause for concern for this kind of sensor and can influence the measurement result significant. However, inductive crosstalk becomes strong suppressed trough the balanced dipole design as already explained, but the capacitive coupling situation influence the linearity of the arc–tan ratio and is difficult to reduce. Since, the receive coils and the excitation share the same Antenna PCB relative closely spaced and due to the relative high excitation frequency, capacitive crosstalk appears from the transmit to the receive coils. A transfer function which describes the coherent capacitive interference between two parallel conductors (see Figure 4) that lie in close proximity is given in [5] and can be used as a simple model for the coupling between transmitter and receiver coils. The transfer function for the coherent interference on any receive coil is given by:

$$\frac{U_{Rx}}{U_{Tx}}(j\omega) = \frac{j\omega C_{12} R_2}{j\omega(C_{12} + C_2)R_2 + 1}, \quad (5)$$

where C_{12} is the capacitance between the transmit and receive coil, which picks up the interference from the transmit coil. Resistance R_2 and capacitance C_2 are parallel–connected, and are the capacitive with respect to ground and ohmic receive coil resistance. From inspection of Equation 5, it is easy to see that in order to minimize the voltage U_{Rx}, due to capacitive crosstalk for all $\omega > 0$, C_{12}, R_2 and U_{Tx} have to be small. However, the coupling capacity C_{12} is difficult to reduce due to the closely spaced transmit and receive coil arrangement, and increasing the distance between the transmit and receive coils will increase the dimensions of the antenna PCB in width and length. The ohmic resistance can be reduced by reducing the number of vias and choosing thicker copper layers.

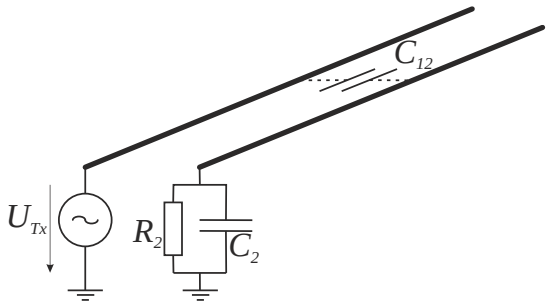

Fig. 4: Simple model describing the electrostatic coupling between two parallel conductors.

This capacitive coupling voltages are illustrated in Figure 5 and Figure 6 for a square wave and a sine wave excitation signal. As we will have gathered, the square wave excitation signal causes significant higher disturbances than the sine wave excitation due to the higher harmonics of the square wave signal fundamental frequency ($3\,f_0$, $5\,f_0$, $7\,f_0$,...). Therefore, a sine signal excitation is recommend.

Theoretically the voltage due to the capacitive coupling appears in phase with the induced voltages $U_{Asin}, U_{Acos}, U_{Psin}$ and U_{Pcos} due to the target oscillating field. An offset voltage appears after demodulation, and thus, the linearity of the arc–tan ratio becomes disturbed [3].

In addition the radiometric transducer design, which means that the position is calculated by the ration of two measurement quantities, offers a strongly reduced influence of mechanical

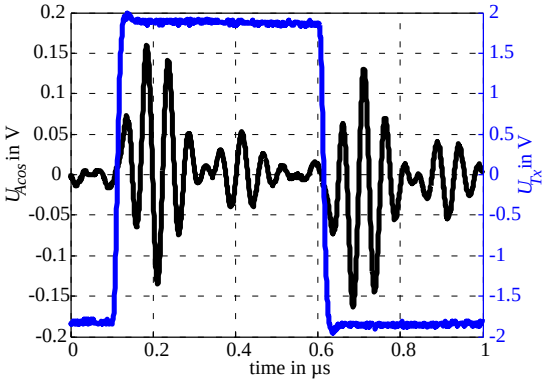

Fig. 5: The measured coupling voltages on the absolute sine receiver coil show voltage transients of 150 mV amplitude. The excitation voltage is approximately a 4 V peak–to–peak 1 MHz square wave signal.

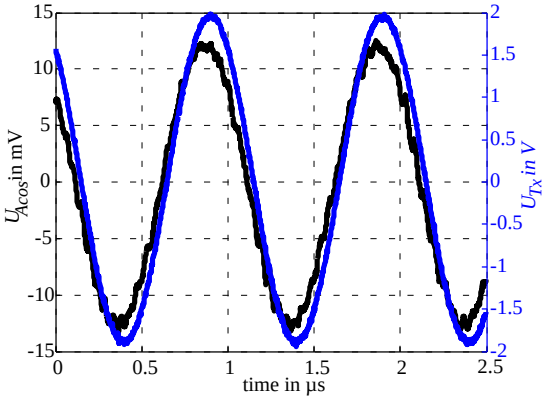

Fig. 6: The measured coupling voltages on the absolute sine receiver coil show voltage transients of approximately 13 mV amplitude. The excitation voltage is a 4 V peak–to–peak 1 MHz sine wave signal

tolerances such as gap variations between target and antenna PCB or other target movements normal to the measurement axis. Therefore, lateral misalignment variations to the measurement axis within ± 10% of the transducer affect the measurement result marginally. The vertical distance between stator and target PCB depends on the application and is usually between 0.5 mm and 3 mm.

The two single period receive coil structures offer absolute position measurement, but the effective measurement length should be limited to 80% of the structure length l_{th} to avoid end effects.

The high inherent resolution allows theoretically resolutions of 0.1% to 0.01% of the antenna length and the absolute linearity of the transducer is between 0.1% and 1% [6].

Figure 7(a) and Figure 7(b) illustrate the receive coil signal behavior after demodulation along the antenna measurement axis. The signals are plotted over the full measurement range ($l_{th} = 390$) mm. A 1 MHz sine signal supplied the transmitter coil when the receive coil signals were measured single ended. Especially the U_Q signal of Figure 7(a) deviates from the ideal cosine curve at $x \in [0, 90) \cup (300, 390]$ mm. These distortions occur due to the interrupted cosine structure at the beginning and end of the antenna PCB (see Figure 3) by the connector at one end and the straight track at the other end. These distortions also affect the linearity of the arctan ratio, but a look up table can be used to straighten out the signals. In Figure 7(a), it is easy to see that the demodulated signal U_{Asin} fits the ideal sine over the full range much better than the demodulated U_{Acos}. The sine structure benefits from its closed structure, which prevents connections by a straight track.

3. SYNCHRONOUS AMPLITUDE DEMODULATION USING UNDERSAMPLING

For obtaining the position of the target, the two absolute receiver signals U_{Asin} and U_{Acos} (Equation 1 and Equation 2) and precise receiver signals U_{Psin} and U_{Pcos} (Equation 3 and Equation 4) have to be demodulated. One basic method utilizing digital demodulation is introduced in this section. The U_{Asin}, U_{Acos}, U_{Psin} and U_{Pcos} signals have to be sampled at the same frequency as the carrier frequency f_0. Undersampling demodulates the receiver signals, and the demodulated and quantized complex envelopes of the amplitude modulated signals can be represented as

$$U_{IA}[i] = \frac{A_R}{2} \sum_{i=0}^{\infty} \sin\left(\frac{2\pi x(t)}{l_{th}}\right) \delta(t - iT), \quad (6)$$

$$U_{QA}[i] = \frac{A_R}{2} \sum_{i=0}^{\infty} \cos\left(\frac{2\pi x(t)}{l_{th}}\right) \delta(t - iT), \quad (7)$$

$$U_{IP}[i] = \frac{A_R}{2} \sum_{i=0}^{\infty} \sin\left(\frac{2\pi x_P(t)}{l_P}\right) \delta(t - iT), \quad (8)$$

$$U_{QP}[i] = \frac{A_R}{2} \sum_{i=0}^{\infty} \cos\left(\frac{2\pi x_P(t)}{l_P}\right) \delta(t - iT), \quad (9)$$

where δ is the Kronecker delta, U_{IA} and U_{QA} the envelope of the absolute receiver signals and U_{IP} and U_{QA} the envelope of the precise receiver signals. To obtain the best possible signal–to–noise ratio the signals U_{Asin}, U_{Acos}, U_{Psin}, and U_{Pcos} have to be sampled simultaneously close to their positive maximum value, synchronized

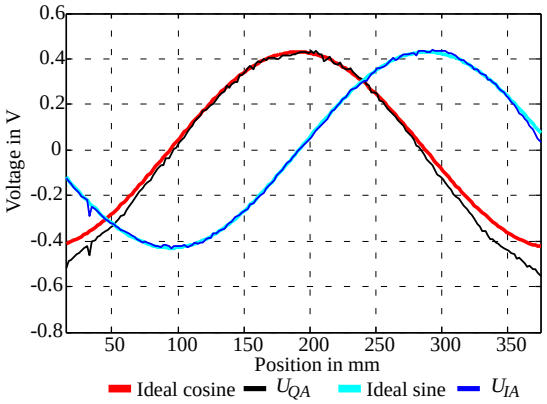

(a) Demodulated output voltages U_{IA} and U_{QA} of the two absolute position receive channels compared to ideal sine and cosine signals.

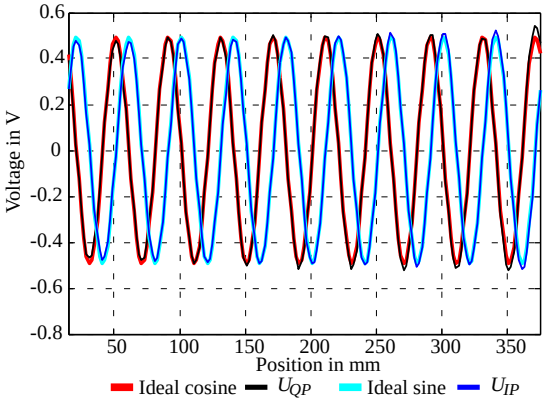

(b) Demodulated output voltages U_{IP} and U_{QP} of the two precise position receive channels compared to ideal sine and cosine signals.

Fig. 7: The demodulated and amplified by a factor 10 measured output voltages of the two absolute (a) and precise (b) position receive channels compared to ideal sine and cosine signals show the behavior of the target resonance circuit along the antenna PCB axis. The target PCB was shifted relatively to the antenna PCB by a linear stage, in 1 mm steps, from the current x–position to the new x–position along the antenna measurement axis. Furthermore, at every position one voltage measurement at the cosine and sine coils were taken. The voltages are not averaged in the figures (a) and (b) and show the demodulated receive coil signals over the full measurement range from 0 mm to 390 mm.

to the carrier frequency f_0. A second order RC–band–pass filter rejects signal components outside the band of interest $f_0 \pm f_B$ before the modulated signals become sampled.

The inverse tangent function of the ratio of absolute structure Equation 6 and Equation 7 and of precise structure Equation 8 and Equation 9 is computed digitally by the DSP to obtain the position. At multiples of $\pi/2$, the computation of $\tan(2\pi x/l_{th})$ has singularities that cause numerical implementation problems. Such singularities are avoided by use of a look–up table (LUT) which uses the symmetrical properties of the tangent and co–tanget functions by correctly selecting the quadrant, octant, and the tangent or cotangent part of $\varphi = 2\pi x/l_{th}$ (see Figure 8). Therefore, the tan– and cotan– functions are always bounded by ± 1. The conditions for selecting the quadrant are given by:

$$Q_i = \begin{cases} i = 1, & \text{if } U_I \geq 0 \wedge U_Q > 0 \\ i = 2, & \text{if } U_I > 0 \wedge U_Q \leq 0 \\ i = 3, & \text{if } U_I \leq 0 \wedge U_Q < 0 \\ i = 4, & \text{if } U_I < 0 \wedge U_Q \geq 0 \end{cases} \quad (10)$$

This gives a full position calculation of the target without any discontinuities at the singular points [7].

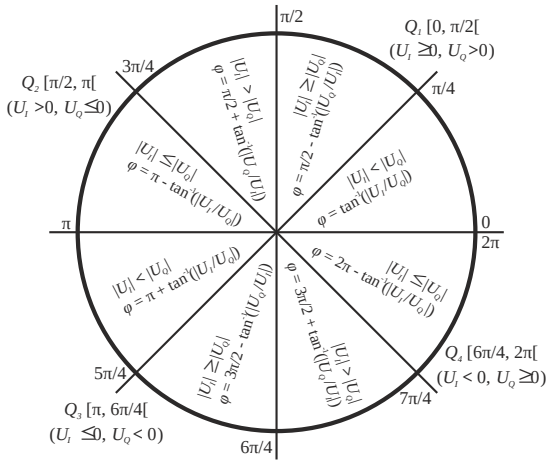

Fig. 8: Arc–tan computation for measurement range $[0, 2\pi x/l_{th}]$ [8].

4. MEASUREMENT SYSTEM AND PRELIMINARY MEASUREMENTS

Figure 9 illustrates the main components of the signal condition electronics for two receive coils. Each receive channel consists of a band–pass filter, an amplifier and a 12–bit ADC. The two coarse and the two fine pitched receive channels become digitalized by a dual channel simultaneous sampling ADC. A DEV–BF537EDA–Lite eval board and the extender board EXT–BF5xx–AD/DA from Bluetechnix provide the digital evaluation electronics. One end of the receiver coils is connected to GND and the other is connected to a second order band–pass filter. The functional block diagram also shows a PWM generated transmit signal, but for the current measurement results and analysis, the

excitation was done by a Agilent 33250A function waveform generator. The PWM excitation has not yet been implemented, but will be done in further development steps. Figure 10 shows the position error along the measurement axis over a range of 350 mm. Approximately 90 % of the theoretical absolute measurement length l_{th} is used by applying precise and absolute structures. Moreover, the preliminary measurement results show that the precise structure position errors are smaller than 0.05 %.

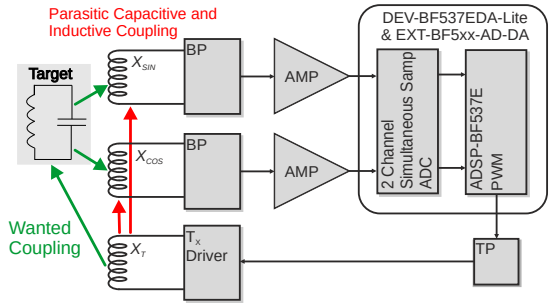

Fig. 9: Functional block diagram of the signal condition electronic for the absolute or precise position receive coils.

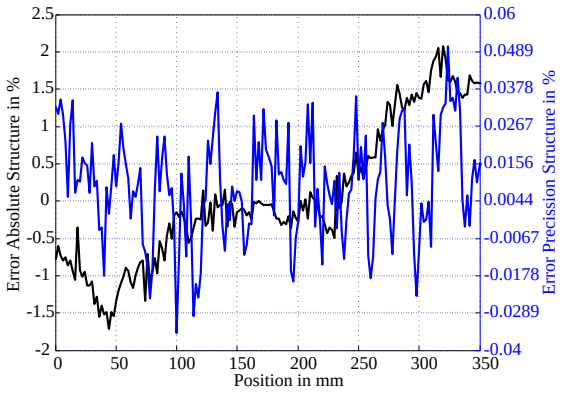

Fig. 10: Full scale position error of the absolute (black line) and precise structure (blue line) along the measurement axis.

5. CONCLUSION

A high-frequency inductive position sensor and a DSP based read–out system has been presented and the sensor operating principle has been explained in detail. Moreover, the concept of sensor signal condition electronics and the measurement results has been explained and presented. The measurement results demonstrate that the sensor, by using an absolute and precise structure, offers a measurement error, with respect to the upper range value, smaller than 0.05 % over 90 % of the theoretical measurement range without further digital signal processing such as angle tracking observer or least square filters. Moreover, the proposed sensor provides high resolution and wide measurement range at reasonable costs.

6. ACKNOWLEDGMENT

The authors acknowledge the financial support for the work presented in this paper by the Austrian Center of Competence in Mechatronics (ACCM).

7. REFERENCES

[1] M. Rahal and A. Demosthenous. An asic front end for planar high-frequency contactless inductive position sensors. *Instrumentation and Measurement, IEEE Transactions on*, 58(9):3021 –3030, sept. 2009.

[2] GB) Doyle Richard Alan (Greenside ZA) Howard Mark Anthony (Worlington GB) James David Alun (Harston GB) Kriet Darran (Foxton GB) Sills Colin Stuart (Cambridge GB) Jones, Ross Peter (Cambridge. Sensing apparatus and method, April 2007.

[3] Mohamad Rahal and Andreas Demosthenous. An integrated signal conditioner for high-frequency inductive position sensors. *Measurement Science and Technology*, 21(1):015203, 2010.

[4] M. Rahal and A. Demosthenous. A synchronous chopping demodulator and implementation for high-frequency inductive position sensors. *Instrumentation and Measurement, IEEE Transactions on*, 58(10):3693 – 3701, oct. 2009.

[5] R. B. Northrop. *Introduction to Instrumentation and Measurements*. CRC Press, 2005.

[6] John Golby. Induktive Weg–Sensoren, Neues Messprinzip ermöglicht maßgeschneiderte Entwicklungen. *Elektronik*, 6:5, Juni 2009.

[7] S. Sarma, V.K. Agrawal, S. Udupa, and K. Parameswaran. Instantaneous angular position and speed measurement using a dsp based resolver-to-digital converter. *Measurement*, 41(7):788 – 796, 2008.

[8] S. Sarma, V.K. Agrawal, and S. Udupa. Software-based resolver-to-digital conversion using a dsp. *Industrial Electronics, IEEE Transactions on*, 55(1):371 –379, jan. 2008.